Article

Size Evaluation of Gold Nanoparticles by UV#vis Spectroscopy

Vincenzo Amendola, and Moreno Meneghetti

J. Phys. Chem. C, **2009**, 113 (11), 4277-4285• DOI: 10.1021/jp8082425 • Publication Date (Web): 24 February 2009

Size Evaluation of Gold Nanoparticles by UV−vis Spectroscopy

Vincenzo Amendola and Moreno Meneghetti*

Department of Chemical Sciences, University of Padova, Via Marzolo 1, I-35131 Padova, Italy

Received: September 16, 2008; Revised Manuscript Received: January 7, 2009

We present a method for the evaluation of the average size of gold nanoparticles based on the fitting of their UV−vis spectra by the Mie model for spheres. The method gives good results using a calibration of the dumping frequency of the surface plasmon resonance and accounting for the presence of nonspherical AuNP in solution by the Gans model for spheroids. It has been successfully applied to free and functionalized gold nanoparticles in various solvents with diameters in the 4−25 nm range. Despite the differences among samples, we found an accuracy of about 6% on the nanoparticles average size with respect to sizes measured by transmission electron microscopy (TEM). Moreover, the fitting model provides other information not available from TEM like the concentration of AuNP in the sample and the fraction of nonspherical nanoparticles, which is particularly useful for measuring aggregation processes. The fitting procedure and models are thoroughly discussed in the text, and the fitting programs are freely accessible on the web.

Introduction

Gold nanoparticles (AuNP) are a very important and frequent tool in nanotechnology, mainly due to their surface plasmon resonance (SPR), their easy surface functionalization or bioconjugation, and their chemical stability and biocompatibility.[1,2] The size, concentration, and, in some cases, aggregation level of AuNP are key points for their applications because they determine optical,[3,4] electrical,[5] chemical,[1] and biological[6,7] properties.

Transmission electron microscopy (TEM) is the most common technique for obtaining accurate data about the average size and size distribution of gold nanoparticles.[8] However, TEM measurements present some disadvantages if a routinely sizing of nanoparticles is needed. In particular, TEM analysis does not allow fast and real-time monitoring of AuNP size, and it does not provide informations about AuNP aggregation and concentration. Moreover, sample preparation is nontrivial and can modify nanoparticles size distribution and morphology,[9,10] for instance, when AuNP are included in solid matrixes or reactive environments.[11]

Other techniques like small-angle X-ray scattering (SAXS),[12−16] differential mobility analysis (DMA),[17] gel electrophoresis (GEP),[18] confocal correlation spectroscopy (CCS),[19] and dynamic light scattering (DLS)[18,20−25] have been used to characterize AuNP solutions. However, the performances of these techniques depend on instrument setup and samples features.[17−19,26] Sample concentration, for instance, determines the measurement time of SAXS and the accuracy of DLS.[12−16,18,19] Surface charge and concentration are limiting factors for the analysis by GEP and DMA.[17,18] Biased diffusion affects DLS in the case of AuNP, which absorb laser light,[19] while CCS is limited to small volumes.[19] Moreover, DMA, GEP, CCS, and DLS determine the hydrodynamic size; they apply only to liquid solutions and do not estimate particles concentration nor discern between isolated or aggregated AuNP.[17−19]

Since the surface plasmon resonance originates an extinction spectrum which depends on the size, shape, and aggregation of AuNP,[1,2,27] UV−vis spectroscopy is a very useful technique which allows estimation of gold nanoparticles size, concentration, and aggregation level. Moreover, UV−vis spectrometers are present in most laboratories, the analysis does not alter the sample, and the registration of the spectrum requires short times. The extinction spectra of AuNP recorded by UV−vis spectroscopy can be analyzed using the Mie theory, once provided the appropriate correction of the metal dielectric constant for the nanoparticle size and the physicochemical environment, as shown by direct measurements on single nanoparticles[28−30] and nanoparticles ensembles.[31−33] Several authors discussed the problem of AuNP sizing by their UV−vis extinction spectra, mainly focusing on the position of the SPR maximum[34−36] or the particles dielectric constant.[37−41] However, in most cases this approach gives unreliable results because the position of the plasmon resonance is affected by multiple factors, like environment dielectric properties,[4,42,43] physical or chemical interactions on particles surface,[44] surface charge,[45] interparticles distance,[28,46] and aggregation.[47]

We previously reported[48,49] that the Mie model for spheres together with the Gans model for spheroids allowed the fitting of AuNP and AgNP extinction spectra, although a partial agreement was found between the average radii measured by TEM and those obtained by the fitting. Here we show that, after calibration of the SPR dumping frequency (Γ) of free gold nanoparticles in water, the size of free or functionalized AuNP in water and other solvents, with diameters between 4 and 25 nm, can be measured with an accuracy of about 6%. Since AuNP can be obtained by laser ablation synthesis in solution (LASiS) as a stable colloidal solution without any surface stabilizer,[48,50] this type of synthesis was useful to monitor the AuNP extinction spectra after addition of thiolated ligands. Moreover the Mie−Gans (MG) fitting model allows estimation of the fraction of nonspherical and aggregated AuNP, which is useful for the quantitative detection of aggregation processes even in their early stages.

We also discuss the possibility of evaluating AuNP standard deviation and size distribution using a log-normal distribution. However, this approach requires the fitting of the interband transitions between 200 and 300 nm, and this is possible, for

* To whom correspondence should be addressed. E-mail: moreno.meneghetti@unipd.it.

10.1021/jp8082425 CCC: $40.75
Published on Web 02/24/2009

TABLE 1: AuNP Solutions

sample	radius* (nm)	standard deviation*	solvent	synthesis type	ligands	absorbance @ the SPR maximum in 2 mm optical path cells	reference
AuNP-1	7.0	61%	H_2O	LASiS	none	0.131	present work
AuNP-2	4.2	28%	H_2O	LASiS + size reduction	none	0.099	present work
AuNP-3	5.0	42%	H_2O	LASiS + size reduction	none	0.090	50
AuNP-4	2.2	22%	H_2O	LASiS + size reduction	none	0.043	50
AuNP-5	8.9	64%	H_2O	LASiS	none	0.233	50
AuNP-1-BSA			see AuNP-1		bovine serum albumine (BSA)	0.142	present work
AuNP-1-ME			see AuNP-1		mercaptoethanol (ME)	0.116	present work
AuNP-2-BSA			see AuNP-2		BSA	0.114	present work
AuNP-2-ME			see AuNP-2		ME	0.086	present work
AuNP-H_2O	10.4	47%	H_2O	LASiS	none	0.401	present work
AuNP-PEG-A			see AuNP-H_2O		mPEG-SH (PEG)	0.423	present work
AuNP-Citrate	4.8	10%	H_2O	Chemical Reduction	citrate	0.174	purchased from sigma (gold colloid G1527)
AuNP-PEG-B			see AuNP-Citrate		mPEG-SH (PEG)	0.148	purchased from sigma (gold colloid G1527)
AuNP-DMSO	2.4	39%	dimethylsulphoxide (DMSO)	LASiS	none	0.099	48
AuNP-THF-1	4.1	61%	tetrahydrofuran (THF)	LASiS	none	0.045	48
AuNP-THF-2	9.1	55%	THF	LASiS + size increase	none	0.109	present work
AuNP-THF-3	3.8	37%	THF	LASiS + size reduction	none	0.079	present work
AuNP-THF:H_2O	12.6	76%	33% THF 66% H_2O	LASiS + size increase	none	0.144	50

* Data from TEM images.

instance, for AuNP obtained by LASiS in water since, usually, stabilizing molecules or solvents different from water absorb in this spectral region. We will show that, for AuNP synthesized by LASiS in water, we obtained log-normal distributions very similar to those measured by TEM.

The fitting programs, freely accessible in the web (see Supporting Information), allow calibration of the model in few steps and can be adapted to other nanoparticles with an SPR in the UV−vis, like silver and copper nanoparticles and noble metals alloys.

Experimental Section

AuNP Samples. In order to set up and test the fitting model we used extinction spectra of various AuNP solutions (Table 1). In eight cases the spectra correspond to solutions which have been prepared by LASiS in water (AuNP-1 and AuNP-H_2O) by LASiS followed by size reduction (AuNP-2) or ligands addition (AuNP-1-BSA, AuNP-1-ME, AuNP-2-BSA, AuNP-2-ME, AuNP-PEG-A). All other samples refer to AuNP solutions whose synthesis has been reported in previously published papers.[48,50] We also used the spectra of aqueous AuNP solutions purchased by Sigma (Gold Colloid G1527) and obtained by chemical reduction synthesis. Table 1 summarizes the average size and relative standard deviation, the solvent, the preparation technique, and, when present, the ligand type for each of the AuNP solution we considered. Figure 1 shows some TEM images representative of AuNP-1, AuNP-2, and AuNP-H_2O samples.

Laser Ablation Synthesis in Solution (LASiS) of AuNP. LASiS of AuNP-1 was carried out with Nd:YAG (Quantel YG981E) laser pulses at 1064 nm (9 ns) focused with a 10 cm focus lens on a gold (99.9%) plate placed at the bottom of a cell containing double-distilled water.[48] We used pulses of about 10−30 J cm^{-2} at a 10 Hz repetition rate.

Size Reduction of AuNP. The AuNP-2 solution was obtained by the size reduction of the AuNP-1 solution. Hence, the gold atom concentration for both AuNP-1 and AuNP-2 is the same. The size reduction was carried out with the second harmonic of the same Nd:YAG laser (532 nm, 9 ns, 10 Hz), with fluences of 120 mJ cm^{-2}, as previously reported.[50] The nanoparticles solution was irradiated for 15 min using a laser beam focused (f = 30 cm) on a 1 cm optical path cell in constant rotation.

Functionalization of AuNP. Functionalization of AuNP obtained by LASiS in the absence of ligands or stabilizing agents occurred in one step, simply by adding the desired molecules to particles solution.

We obtained solutions of AuNP-1-BSA and AuNP-2-BSA by mixing a 0.5 mM aqueous solution of bovine serum albumin

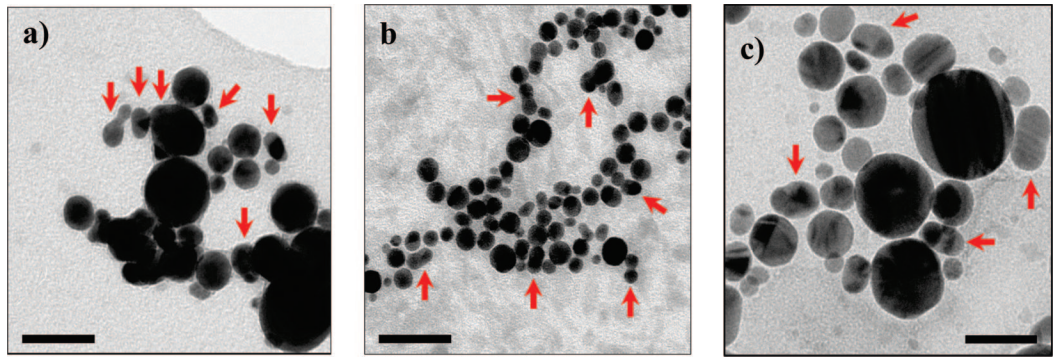

Figure 1. TEM images of samples AuNP-1 (a), AuNP-2 (b), and AuNP-H_2O (c). Scale bar is 40 nm. For details see Table 1. Red arrows indicate some examples of nonspherical AuNP.

(BSA; in powder, fatty acid free, purchased from Sigma-Aldrich) to AuNP-1 and AuNP-2 solutions. The final BSA concentration was 0.05 mM in both cases.

We obtained solutions of AuNP-1-ME and AuNP-2-ME by mixing a 1 mM aqueous solution of 2-mercaptoethanol (ME, >99% pure, purchased from Sigma-Aldrich) to AuNP-1 and AuNP-2 solutions. The final ME concentration was 0.1 mM in both cases.

We obtained a solution of AuNP-PEG-A by mixing a 0.2 mM aqueous solution of thiolated poly ethylene-glycol (PEG hereafter mPEG-SH MW 5000, purchased from Laysan Bio Inc.) to AuNP−H_2O solution. The final PEG concentration was 1 μM.

We obtained a solution of AuNP-PEG-B by mixing a 0.2 mM aqueous solution of PEG to AuNP−Citrate solution. The final PEG concentration was 1 μM.

Characterization of AuNP. All AuNP solutions were characterized by UV−vis spectroscopy with a Varian Cary 5 spectrometer in 2 mm optical path cells and by transmission electron microscopy (TEM) at 300 kV with a JEOL JEM 3010 microscope equipped with a Gatan Multiscan CCD Camera model 794. TEM samples were prepared by depositing some gold colloid drops on a copper grid covered with a holey carbon film.

Mie−Gans Fitting Model

Morphological features of AuNP and their physico−chemical environment influence the SPR and the corresponding extinction spectra. Typically, the UV−vis spectrum of spherical nonaggregated gold nanoparticles is composed by a band around 520 nm, due to the SPR, plus an absorption edge at shorter wavelengths due to interband transitions of d-band electrons.[27]

The extinction cross section of spherical AuNP can be successfully calculated using the Mie model for compact spheres (calculated spectra can be seen in Figure S1a in the Supporting Information). The Mie model is based on the resolution of the Maxwell equations in spherical coordinates using the multipoles expansion of the electric and magnetic fields and accounting for the discontinuity of the dielectric constant between the sphere and the surrounding medium.[27] The Mie model expressions of extinction cross section σ_{ext} for a single sphere of radius R are[27]

$$\sigma_{ext} = \frac{2\pi}{|\bar{k}^2|}\sum_{L=1}^{\infty}(2L+1)Re[a_L + b_L] \quad (1.a)$$

$$a_L = \frac{m \cdot \psi_L(mx) \cdot \psi_L'(x) - \psi_L'(mx) \cdot \psi_L(x)}{m \cdot \psi_L(mx) \cdot \eta_L'(x) - \psi_L'(mx) \cdot \eta_L(x)} \quad (1.b)$$

$$b_L = \frac{\psi_L(mx) \cdot \psi_L'(x) - m\psi_L'(mx) \cdot \psi_L(x)}{\psi_L(mx) \cdot \eta_L'(x) - m\psi_L'(mx) \cdot \eta_L(x)} \quad (1.c)$$

$$m = \frac{n(R)}{n_m} \quad (1.d)$$

$$x = |\bar{k}|R \quad (1.e)$$

where k is the incident photon wavevector, Ψ_L and η_L are the spherical Riccati−Bessel functions, n_m is the real refraction index of the nonabsorbing surrounding medium, and $n(R)$ is the complex refraction index of the gold sphere of radius R. For all calculations we set the multipolar order $L = 3$. The x parameter determines if the sphere is in quasistatic (dipolar, $R \ll \lambda$ then $x \ll 1$) or dynamic regime (multipolar, $R \approx \lambda$).[27] This type of size dependence is called the extrinsic size effect or retardation effect and is a bare electromagnetic phenomena, contrary to the intrinsic size effect due to the dependence of metal dielectric constant on the size.[27] In the case of gold AuNP, the extrinsic size effect is found for diameters above 30 nm and preponderant for 50 nm.[27] The intrinsic size effect appears in the SPR below that limit, when the conduction electrons mean free path (~45 nm for Au) becomes comparable to the particle size and electron scattering at the particle surface becomes an important component of the SPR width.[27] The dielectric constant can be corrected for size using a R-dependent relaxation frequency $\Gamma(R)$ by introduction of the following relationship[27,31,44]

$$\Gamma(R) = \Gamma_\infty + A\frac{\upsilon_F}{R} \quad (2.a)$$

where Γ_∞ is the bulk metal value, υ_F is the Fermi speed, and A is an empirical parameter. We will show in the following sections that A is indispensable to account for all other factors affecting SPR width as surface interactions or the uncertainty on the bulk gold dielectric constant. In particular, by correction of A one can account for the chemical interface dumping (CID) effect which occurs when strongly bound ligands (i.e., thiols) are present on the AuNP surface.[27,44,51−53] For our calculations, we modified the value of A as described in the section on the calibration of the fitting model.

On the assumption that only the free electron behavior is affected by the size of nanoparticles, $\varepsilon(\omega,R)$ can be expressed in the following way[27]

$$\varepsilon(\omega,R) = \varepsilon_\infty(\omega) + \left[\omega_P^2\left(\frac{1}{\omega^2+\Gamma_\infty^2} - \frac{1}{\omega^2+\Gamma(R)^2}\right)\right] + i\left[\frac{\omega_P^2}{\omega}\left(\frac{\Gamma(R)}{\omega^2+\Gamma(R)^2} - \frac{\Gamma_\infty}{\omega^2+\Gamma_\infty^2}\right)\right] \quad (2.b)$$

where $\varepsilon_\infty(\omega)$ is the dielectric function of bulk gold.

Using eq 2.b and the Mie model, one can see that the SPR width increases for decreasing sizes in the 4−28 nm interval (Supporting Information, Figure S1a) and that the extinction cross section depends linearly on particles volume (Supporting Information, Figure S1b).

Direct measurements on single AuNP demonstrated that both extrinsic and intrinsic size effects can be estimated by the Mie model when eq 2.b is adopted for the dielectric constant.[28−30]

However, for AuNP sizes smaller than about 2−4 nm, depending on surface coating, quantum size effects influence the shape and position of the SPR and also the behavior of the d-band electrons becomes size dependent.[27,37] Therefore, the Mie model with the above recalled correction of the dielectric constant is appropriate when particles have sizes larger than about 4 nm, while it fails in estimating the blue shift and shape of SPR, which are experimentally observed on particles smaller than about 4 nm.[37,39,52,53]

As previously reported, [27,48−50] we found in several cases that the Mie model alone is not adequate for fitting of experimental UV−vis spectra at wavelengths above 550 nm, where the absorption is larger than that calculated. Indeed, the Mie model accounts only for spherical particles, while AuNP in solution can have different structures. TEM images, although only in part representative of particles aggregation in solution, often show the presence of cigarlike shapes and small aggregates made by few AuNP fused together (see arrows in Figure 1), and this can explain the observed deviations of the experimental spectra above 540 nm.[28,46,48,50] In the case of AuNP obtained by LASiS, due to the absence of stabilizing molecules, small aggregates of AuNP or slightly spheroidal nanoparticles are frequent in

TEM pictures (Figure 1). However, aggregates and spheroids can be found also in AuNP solutions obtained by chemical reduction and after functionalization of weakly (i.e., citrate) stabilized particles.

Since aggregation can involve two or more particles and most isolated particles with nonspherical shape basically are low aspect ratio spheroids, one can account for the contribution of small aggregates and nonspherical particles to the overall extinction spectra using the Gans model, that is the Mie theory extension to particles with spheroidal shape.[27,36,43] In fact, UV−vis spectra of spheroidal nanoparticles have two characteristic absorption bands: one at the same frequency of spherical particles due to plasmon excitation along the shorter axes and the other red shifted and usually more intense with respect to the first due to excitation along the longer axis.[43] This last feature can account for the absorption above 550 nm that we observed.

Therefore, we completed the fitting of experimental UV−vis spectra including the contribution of nonspherical particles by means of the Gans model. For a prolate spheroid of aspect ratio a/b, where b is the smaller axis ($a > b = c$), the σ_{ext} averaged over all possible orientation in space is[27,43]

$$\sigma_{ext} = \frac{2\pi V \varepsilon_m^{3/2}}{3\lambda} \sum_j \frac{\frac{1}{P_j^2}\varepsilon_2(\omega, R)}{\left(\varepsilon_1(\omega, R) + \frac{1-P_j}{P_j}\varepsilon_m\right)^2 + \varepsilon_2(\omega, R)^2} \tag{3.a}$$

$$P_a = \frac{1-e^2}{e^2}\left[\frac{1}{2e}\ln\left(\frac{1+e}{1-e}\right) - 1\right] \tag{3.b}$$

$$P_b = P_c = \frac{1-P_a}{2} \tag{3.c}$$

$$e = \sqrt{1-\left(\frac{b}{a}\right)^2} \tag{3.d}$$

where λ is the wavelength of incoming photons, ϵ_m is the matrix real dielectric constant, $V = (4\pi/3)ab^2$ is the volume, and e is the eccentricity of the spheroid.

We accounted for particles with different shapes as spheroidal particles with a distribution of aspect ratios, and we assumed a Gaussian probability $G(a/b)$ centered at a/b=1 for such a distribution[43,48]

$$G(a/b) = \frac{1}{S_G\sqrt{2\pi}}\exp\left[-\frac{(a/b-1)^2}{2S_G^2}\right] \tag{4}$$

where $a/b > 1$ and S_G is the standard deviation, which indicates that 68% of spheroidal particles have a/b smaller than $1 + S_G$. The Gaussian probability was chosen because random processes are responsible for aggregations.

Despite the size and shape distribution contained in each sample, the Mie−Gans (MG) models with the above-discussed assumptions allowed the optimal fitting of experimental UV−vis spectra using only three parameters: (i) the average radius of the nanoparticles (R), (ii) the standard deviation (S_G) of the a/b Gaussian distribution, and (iii) the fraction of spherical to spheroidal gold nanoparticles (or Spheres % hereafter). The geometrical average of the spheroids semiaxes was considered to be equal to the average spheres radius, that is, $R = \sqrt[3]{ab^2}$, hence considering that all the particles have the same volume and avoiding introduction of other parameters.[4,48]

Initialization of the MG model consisted of a rough estimation of the average radius by fitting the 300−950 nm spectral region with the Mie model only, whereas the final average radius R, the Spheres %, and the spheroids a/b distribution S_G were obtained by fitting the same wavelength interval with the contributions coming from both the Mie model for spheres and the Gans model for nonspherical particles. The best fitting for each spectrum is achieved by varying R of 0.1 nm, S_G of 0.05, and the Spheres % of 0.5% in their intervals. A χ^2 fitting on a point every 5 nm was used for calculation of the best spectra, which were normalized on the SPR maximum (SPR_{MAX}). Calculated curves were allowed to shift 1 point, if necessary, to improve the matching with the position of the experimental SPR_{MAX}. In Scheme 1 the MG fitting procedure is sketched, and a copy of the MG fitting program can be downloaded freely from the web (see Supporting Information).

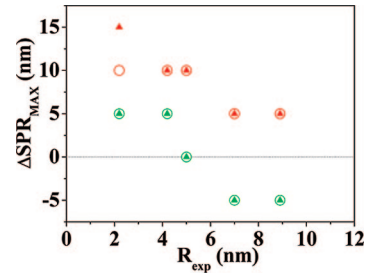

Figure 2. Difference between calculated and experimental SPR maximum (ΔS PA_{MAX}) in the case of Mie fitting (hollow circles) and MG fitting (full triangles) using the dielectric constant tabulated by Johnson and Christy (red) and Palik (green). Positive values mean that calculated spectra are red shifted with respect to experimental spectra. Fitting refers to samples of AuNP in water with average radii of 7.0 (AuNP-1), 4.2 (AuNP-2), 5.0 (AuNP-3), 2.2 (AuNP-4), and 8.9 nm (AuNP-5).

Scaling the values of the calculated spectra to the experimental ones allows determination of the concentration of the nanoparticles according to

$$\mathrm{Abs}(\omega) = -\mathrm{Log}_{10}[\exp[-dN\sigma_{ext}(\omega)]] \tag{5}$$

where Abs is the absorbance, d is the optical path, and N is the number of AuNP for unit volume with average extinction cross section σ_{ext}.

Discussion and Results

a. Dielectric Constant of Bulk Gold. In terms of the shape and position of the plasmon band, the agreement between calculated and experimental SPR also depends on the accuracy of the bulk gold dielectric function ($\varepsilon_\infty(\omega)$) used in eq 2.b.[27] Usually calculation of plasmonic properties of gold nanostructures consider the $\varepsilon_\infty(\omega)$ measured by Johnson and Christy.[54]

However, we observed a systematic red shift (see Figure 2) of the SPR calculated with both the Mie (red hollow circles) and the Mie−Gans (MG) (red triangles) models for samples of AuNP without stabilizing molecules in water (Table) using this dielectric constant. We found, on the other hand, that, using the $\varepsilon_\infty(\omega)$ values tabulated for gold by Palik in its *Handbook of Optical Constants of Solids*,[55] the agreement in the SPR position was improved with both the Mie (green hollow circles in Figure 2) and MG (green triangles) models. A similar result was also previously found for silver nanoparticles, whose SPR was reproduced better with the Palik dielectric constant than with the Johnson and Christy one.[49,56] Hence, in the following we present only fittings obtained with Palik values for $\varepsilon_\infty(\omega)$ instead of the commonly used Johnson and Christy values.

Tables of the $\varepsilon_\infty(\omega)$ used for the fittings are provided in the file SPRFit.zip (see Supporting Information).

SCHEME 1: MG Fitting Procedure

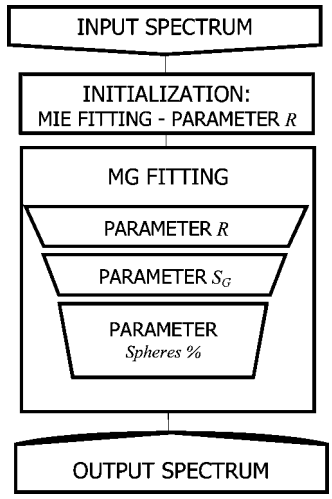

b. Comparison between Mie and Mie−Gans Fittings. As discussed previously, the Mie model accounts for spherical AuNP; therefore, it is unable to reproduce the plasmonic spectrum, above 550 nm, of solutions with a non-negligible fraction of nonspherical shapes (red circles in Figure 3a). On the contrary, the MG fitting provides a better agreement also at wavelengths larger than 550 nm (green triangles in Figure 3a and inset). Figure 3b shows in detail the two contributions to the best MG fitting of the AuNP-1 experimental spectrum. The first one is relative to spherical AuNP calculated with the Mie model (red hollow circles), which accounts for the main part of the SPR around 520 nm. The second one is relative to spheroidal AuNP with a Gaussian distribution of aspect ratios calculated with the Gans model (blue hollow triangles) and accounts for the plasmonic absorption around 600 nm. The resultant aspect ratio distribution is reported in the inset of Figure 3b.

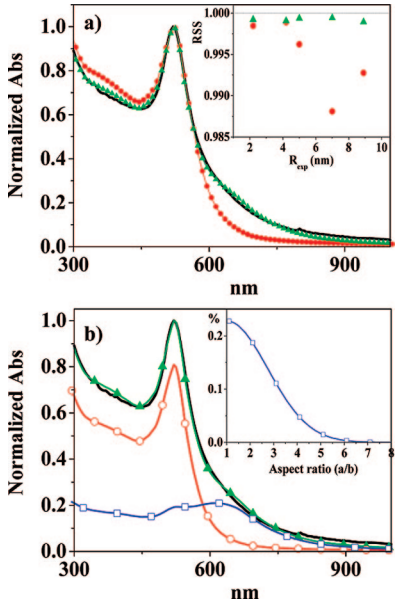

Figure 3. (a) Mie (red circles) and MG (green triangles) fitting of the experimental spectrum of AuNP-1 solution (particles with average size of 7.0 nm). (Inset) RSS (root summed square) for the Mie (red circles) and MG (green triangles) fittings referred to samples of AuNP in water with average radii of 7.0 (AuNP-1), 4.2 (AuNP-2), 5.0 (AuNP-3), 2.2 (AuNP-4), and 8.9 nm (AuNP-5). (b) Decomposition of the MG fitting (green triangles) of AuNP-1 experimental spectrum (black line) by the spherical particles Mie contribution (red hollow circles) and the spheroidal particles contribution with a Gaussian distribution of aspect ratios calculated with the Gans model (blue hollow squares). (Inset) Gaussian distribution of aspect ratios. Fitting parameters are reported in Table 2.

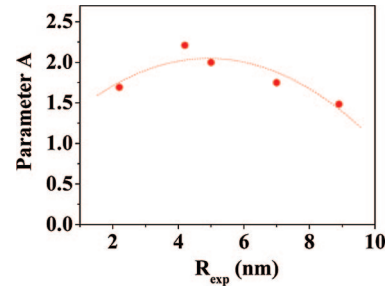

Figure 4. Parameter *A* corrected according to eq 6.a (red circles) for samples reported in Table 2 and the parabolic fit of eq 6.b (dashed line).

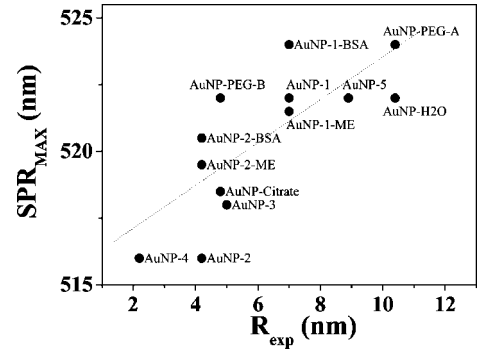

Figure 5. Plot of the wavelength at the SPR maximum (SPR_{MAX}) versus AuNP radius for all aqueous solutions.

c. Calibration of the Mie−Gans Model. The Mie−Gans fitting model as well as the Mie model are inaccurate in estimating the average radius of AuNP, as obtained by TEM images, when the *A* parameter is 1.[27,29,30,44,52] However, results of Figure 2 show that calculated spectra of AuNP are strongly influenced by the values of the dielectric constant and suggests that a calibration of $\varepsilon(\omega,R)$ can be used to improve the agreement with experimental results. Several authors reported the correction of gold dielectric constant to obtain better agreement between calculated and experimental spectra of gold nanostructures.[36,38−41,56−58] For the calibration of $\varepsilon(\omega,R)$ we used eq 2.a because it is an empirical relationship and *A* can be adjusted to obtain a better estimation of particles size. We corrected *A* rescaling its value according to[27,44]

$$A_{corr} = A\frac{R_{exp}}{R_{calc}} \qquad (6.a)$$

where R_{exp} is the TEM measured average AuNP radius and R_{calc} is that calculated by the MG fitting of the experimental UV−vis spectrum using $A = 1$.

Figure 4 show the results obtained for the five samples of free AuNP in water reported in Table 2. The following parabolic fit was used to account for the dependence of *A* on particles radius *R*

$$A = 1.09 + 0.39R - 0.04R^2 \qquad (6.b)$$

Several authors reported that *A* changes its value for AuNP having similar physicochemical environment but different sizes, in particular ranging from about 0.5 to about 2.[28−30,44,51,52]

TABLE 2: MG Fitting Results for AuNP Solutions in Water

	from TEM images			MG fitting					
sample	radius (nm)	standard deviation	Abs @ SPA_{MAX}	R (nm)	ΔR	Spheres %	S_G	σ_{ext} @ SPA_{MAX} (m^{-2})	AuNP Conc. (M)
AuNP-1	7.0	61%	0.131	7.4	+6%	77.0%	1.75	1.1 E-16	2.2 E-9
AuNP-2	4.2	28%	0.099	3.8	−10%	97.5%	1.25	1.2 E-17	1.6 E-8
AuNP-3	5.0	42%	0.090	5.1	+2%	94.0%	2.85	3.2 E-17	5.4 E-9
AuNP-4	2.2	22%	0.043	2.2	0%	94.0%	1.75	1.9 E-18	4.3 E-8
AuNP-5	8.9	64%	0.233	8.9	0%	76.0%	1.30	2.2 E-16	2.0 E-9

TABLE 3: MG Fitting Results for AuNP Solutions in Various Solvents and Various Surface Stabilization

	from TEM images			MG fitting					
sample	radius (nm)	standard deviation	Abs @ SPA_{MAX}	R (nm)	ΔR	Spheres %	S_G	σ_{ext} @ SPA_{MAX} (m^{-2})	AuNP Conc. (M)
AuNP-DMSO	2.4	39%	0.099	2.3	−4%	84.5%	2.05	2.9 E-18	6.6 E-8
AuNP-THF-1	4.1	61%	0.045	4.6	+12%	61.0%	1.30	2.6 E-17	3.3 E-9
AuNP-THF-2	9.1	55%	0.109	9.7	+7%	68.0%	1.65	3.4 E-16	6.1 E-10
AuNP-THF-3	3.8	37%	0.079	3.8	0%	62.0%	1.85	1.3 E-17	1.1 E-8
AuNP-THF:H_2O	12.6	76%	0.144	12.6	0%	50.0%	1.35	7.7 E-16	3.6 E-10
AuNP−H_2O	10.4	47%	0.401	10.1	−3%	70.5%	0.70	3.6 E-16	2.2 E-9
AuNP-PEG-A	10.4	47%	0.423	9.8	−6%	78.0%	0.90	3.2 E-16	2.5 E-9
AuNP-1-BSA	7.0	61%	0.142	6.8	−3%	78.0%	1.75	8.4 E-17	3.3 E-9
AuNP-1-ME	7.0	61%	0.116	6.7	−4%	79.5%	1.60	8.0 E-17	2.8 E-9
AuNP-2-BSA	4.2	28%	0.114	4.0	−5%	98.5%	2.75	1.4 E-17	1.6 E-8
AuNP-2-ME	4.2	28%	0.086	3.1	−26%	97.0%	2.60	5.9 E-18	2.8 E-8
AuNP-Citrate	4.8	10%	0.174	4.3	−10%	97.0%	3.15	1.8 E-17	1.9 E-8
AuNP-PEG-B	4.8	10%	0.148	5.0	+4%	78.0%	1.25	3.0 E-17	9.6 E-9

Replacing $A = 1$ with eq 6.b in the MG model we found an error of 0−10% between R_{exp} and R_{calc} (Table 2). In Table 2 we report all the fitting parameters (R, Spheres %, and S_G), the average extinction cross section for single AuNP at the SPR maximum (σ_{ext} @ SPA_{MAX}), and the resultant estimated AuNP concentration (AuNP Conc.). The comparison of calculated and experimental spectra is reported in Figure S2a−e for samples AuNP-1−5. As previously reported,[48,50] AuNP obtained by LASiS (AuNP-1 and AuNP-5) have a significant fraction of nonspherical particles, which appreciably decreases after the size reduction procedure (AuNP-2, AuNP-3, and AuNP-4).

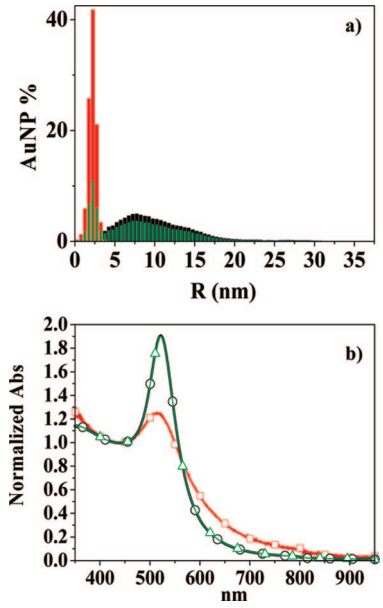

Figure 6. (a) Histograms of AuNP radii for sample AuNP-4 (average radius 2.2 nm, red bars), AuNP−H_2O (average radius 10.4 nm, black bars), and a sample composed by 50% of AuNP-4 and 50% of AuNP−H_2O (green bars). (b) UV−vis spectra of sample AuNP-4 (average radius 2.2 nm, red squares), AuNP−H_2O (average radius 10.4 nm, black circles), and a sample composed by 50% in number of AuNP-4 and 50% of AuNP−H_2O (green triangles). All spectra are normalized at 450 nm for a clearer comparison.

d. General Application of the Mie−Gans Model to AuNP Solutions. Calibration of the Mie−Gans model exploited ligand-free AuNP with different sizes in solutions of pure water; hence, we checked the validity of this model with other AuNP solutions.

Concerning solutions of AuNP in pure solvents like water, dimethyl sulfoxide (DMSO), and tetrahydrofuran (THF) or mixed THF:H_2O obtained by LASiS and/or size reduction/increase, the fitting has an accuracy of about 4% (see Table 3). This result indicates that the accuracy of the calibrated MG model is independent of the solvent type.

Since the conjugation of AuNP to thiolated ligands and large biomolecules influences their SPR,[27] we tested the MG fitting model in the case of free AuNP obtained by LASiS in water and functionalized with bovine serum albumin (BSA), mercaptoethanol (ME), and thiolated poly(ethylene-glycol) (PEG). Coating the AuNP surface with BSA, ME, and PEG produced the red shift and broadening of the SPR (see Supporting Information, Figure S3). The red shift of the SPR can derive from the increase in the dielectric constant around particles surface,[27] while the SPR broadening indicates that surface

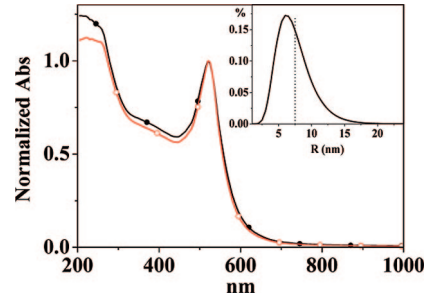

Figure 7. Calculated extinction spectra for two ideal solutions composed by 100% identical spherical AuNP with a radius of 7.5 nm (red hollow circles) and 100% spherical AuNP with an average radius of 7.5 nm and a log-normal size distribution with $R_C = 7$ nm, $w = 0.35$, and resultant standard deviation of 36% (black full circles). Inset shows the log-normal size distribution. We considered $A = 1.827$ for all radii and water matrix for Mie model calculations. Spectra were normalized on the SPR_{MAX}.

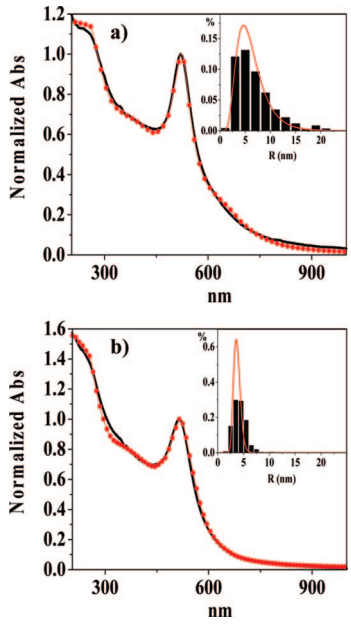

Figure 8. LNMG fitting (red circles) of AuNP-1 (a) and AuNP-2 (b) experimental spectra (black lines). Inset shows the TEM measured experimental size histograms (black bars) and the log-normal size distribution estimated by the LNMG fitting (red lines). Fitting parameters are $R_C = 5.8$ nm, $w = 0.45$, $S_G = 1.7$, Spheres % = 58% for AuNP-1 and $R_C = 3.7$ nm, $w = 0.15$, $S_G = 2.5$, Spheres % = 98.0% for AuNP-2.

ligands provided new relaxation channels for plasmon excitation.[27,44] For functionalized AuNP samples reported in Table 3, the MG model underestimated the average size of 3−5%, except for AuNP-2-ME, where the error was 26% (evaluated average radius of 3.1 nm versus the TEM estimated value of 4.2 nm). In this case size underestimation is the effect of the SPR broadening produced by surface ligands.[27,44] In fact, AuNP-2-ME sample consists of relatively small AuNP ($R = 4.2$ nm), with a large fraction of surface atoms, and of a densely packed surface ligand (mercaptoethanol), which is bound to the gold surface by the covalent S−Au bonds. Changes in SPR are more evident for AuNP-2-ME than for samples with large particles like AuNP-1-ME and AuNP-PEG-A or samples having ligands with low surface density of covalent bonds like AuNP-2-BSA. This finding is in accord with the paper of Garcia et al.,[52] where they show that the SPR dumping frequency depends on the interaction strength of the capping layer on AuNP surface and is more important for smaller radii.

The preparation method of AuNP determines the standard deviation and percentage of nonspherical particles in the sample;[1] therefore, we tested the MG model with commercial citrate-stabilized AuNP obtained by chemical reduction in water, having 10% of standard deviation. The size of AuNP−Citrate was estimated by the MG model with an error of 10%. When the same particles were coated with PEG the size was estimated only with a 4% error. Moreover, the fittings estimated the 3% of nonspherical AuNP for citrate-stabilized commercial particles and 22% of spheres for same particles after coating with PEG, which confirms that ligand addition can affect the stability of citrate-stabilized AuNP.

In summary, the calibrated MG model estimated the average size of AuNP with an accuracy of about 6%, ranging from 0% to 12%, except for the above-discussed AuNP-2-ME sample, where the error was 26%. One must point out that the same results cannot be obtained by measuring of the SPR maximum. In fact, in Figure 5 we report the wavelength at the SPR maximum for all AuNP solutions in water and it is possible to see that solutions of AuNP having the same average radii, when coated with different ligands, have a different position of the SPR_{MAX} and that solutions of AuNP with different average sizes can have the SPR_{MAX} at the same wavelength.

e. Application of the Mie−Gans Model to Polydispersed AuNP Solutions. When considering a polydispersed AuNP sample with more than one maximum in the distribution of particles radii, like that of Figure 6a, one finds that the corresponding UV−vis spectrum is dominated by the fraction of particles with larger size (Figure 6b). In fact UV−vis spectra provide averaged information about AuNP solutions and the average is weighted by particle volumes, since σ_{ext} is linearly dependent on R^3 (Supporting Information, Figure S1b). For the sample of Figure 6, the MG fitting estimated the average radius with an error of +60% ($R = 10.1$ nm versus an average radius of 6.3 nm). Histograms of gold atoms percentage (Supporting Information, Figure S4b) confirm that the volume contribution of the fraction of small particles is negligible, explaining why their contribution to the UV−vis spectrum is undetectable. Hence, in the case of highly polydispersed AuNP samples, the MG fitting of UV−vis spectra can overestimate the average size.

f. Evaluation of AuNP Size Distribution. The MG model provides information about AuNP samples, but it does not provide data about the size distribution. In principle, estimation of the size distribution of a given monodispersed AuNP solution from its UV−vis spectrum is possible. Figure 7 shows the spectra calculated for the ideal case of monodispersed gold nanoparticles in water having the same radius $R = 7.5$ nm (red hollow circles) and that calculated for the case of gold nanoparticles with average radius $R = 7.5$ nm and a standard deviation of 36% (black circles) due to a log-normal distribution of sizes (inset of Figure 7). Almost no differences are detected after 500 nm in the SPR region, while the spectra are different mainly around 200−270 nm. The spectral region around 200−270 nm is related to gold interband transitions and depends directly on the gold atoms concentration in the sample.[27] We can show that this spectral region can be exploited to obtain information about the AuNP size distribution and estimate the standard deviation on the average radius. Clearly this is possible only in cases where this spectra region is free of absorptions of other molecules like ligands or solvents, and AuNP obtained by LASiS in water offer this opportunity. In this case nanoparticles are obtained with a log-normal size distribution;[48−50,58−62] hence, we modified the MG model replacing the parameter R, i.e., the average spheres radius, with two new parameters necessary to describe a log-normal distribution of spherical particles radii, namely, the center of the distribution R_C and its width w. In this log-normal Mie Gans (LNMG) fitting model $\sigma_{ext}(\omega,R)$ is weighted by the probability given by the log-normal distribution $LN(R)$ according to the following expressions

$$LN(R) = \frac{1}{\sqrt{2\pi}(wR)}\exp\left[-\frac{1}{2w^2}\left(\log\left[\frac{R}{R_C}\right]\right)^2\right] \qquad (7.a)$$

$$\sigma_{ext}(\omega) = \frac{\int_{R=0}^{R=\infty} LN(R)\sigma_{ext}(\omega,R)\mathrm{d}R}{\int_0^\infty LN(R)\mathrm{d}R} \qquad (7.b)$$

The LNMG fitting model depends on four parameters: (i) the center of the log-normal radii distribution R_C; (ii) the width of the log-normal radii distribution w; (iii) the fraction of spherical to spheroidal gold nanoparticles (Spheres %, same as for MG fitting), and (iv) the standard deviation of the a/b Gaussian distribution (S_G, same as for MG fitting). In this model

we only used an average value of the parameter A ($A = 1.827$) since the log-normal distribution also considers nanoparticles with very large diameters which are not included in the calibration curve of Figure 4.

The LNMG fitting procedure is the same as the MG fitting (see Scheme S1 in the Supporting Information) except for the fitted spectral region which extends from 205 to 950 nm and not, as usual, from 300 to 950 nm. The LNMG fitting program is provided as Supporting Information.

As an example, we considered the LNMG fitting of samples AuNP-1 and AuNP-2 (see Figure 8). The insets show the good comparison between the log-normal distributions obtained by the fittings (continuous line) and that obtained by TEM measurements. In fact, calculated average radii are found to be 6.4 and 3.7 nm versus the experimental values of 7.0 and 4.2 nm for AuNP-1 and AuNP-2, respectively, and calculated standard deviations of 48% and 15% instead of the experimental values of 61% and 28% for AuNP-1 and AuNP-2, respectively (see Table S1 in the Supporting Information).

The LNMG fitting calculated an average extinction cross section for single AuNP at the SPA_{MAX} of 1.2×10^{-16} m^2 (AuNP Conc. 2.1×10^{-9} M) and 1.3×10^{-17} m^2 (AuNP Conc. 1.6×10^{-8} M) for AuNP-1 and AuNP-2, respectively, while values calculated by the MG fitting are respectively 1.1×10^{-16} m^2 (AuNP Conc. 2.2×10^{-9} M) and 1.2×10^{-17} m^2 (AuNP Conc. 1.5×10^{-8} M). This suggests that the concentration of particles estimated by the MG model is scarcely affected by the size distribution of AuNP also for samples with standard deviations as high as 48%.

Conclusions

Size, concentration, and aggregation level of gold nanoparticles are key points for their applications. We presented in detail a method for estimating these properties by UV−vis spectroscopy, based on the fitting of experimental spectra with the Mie and Gans models. Calibration of the SPR dumping frequency Γ allowed an accuracy on the evaluation of average particles size of about 6% for different types of AuNP solutions with diameters between 4 and 25 nm. A model for the estimation of the size distribution of AuNP by extending the fitting of the UV−vis spectra down to 200 nm range was also shown to give good results.

Through the calibration procedure and the fitting program, which is provided on the web (see Supporting Information), the MG fitting can be adjusted to the case of other nanoparticles with a characteristic SPR in the UV−vis like silver, copper, and noble metals alloys.

Acknowledgment. We thank Prof. S. Polizzi for TEM images and Prof. F. Stellacci, E. Penzo, J. Y. Kim, and G. Marcolongo for technical help and useful discussions. Financial support by the Italian Ministry of Universities and Research (PRIN prot. 2006034372) and the University of Padova (PRAT prot. CPDA063353) is acknowledged.

Supporting Information Available: Mie model simulations; fittings of AuNP solutions; spectra of functionalized AuNP; particles and gold atoms distributions of the polydispersed AuNP sample; sketch of the LNMG fitting procedure; zip file (SPRFit.zip) containing the fitting programs MG Fit 1.0 and LNMG Fit 1.0 (running under Wolfram Mathematica 4.0 or later versions) and bulk gold dielectric constants can be download freely at http://www.chimica.unipd.it/vincenzo.amendola. This material is available free of charge via the Internet at http://pubs.acs.org.

References and Notes

(1) Daniel, M. C.; Astruc, D. *Chem. Rev.* **2004**, *104*, 293–346.
(2) Xia, Y.; Halas, N. J. *MRS Bull.* **2005**, *30*, 338–348.
(3) Rosi, N. L.; Mirkin, C. A. *Chem. Rev.* **2005**, *105*, 1547–1562.
(4) Jain, P. K.; Lee, K. S.; El-Sayed, I. H.; El-Sayed, M. A. *J. Phys. Chem. B* **2006**, *110*, 7238–7248.
(5) Marinakos, S. M.; Shultz, D. A.; Feldheim, D. L. *Adv. Mater.* **1999**, *11*, 34–37.
(6) Chithrani, B. D.; Chan, W. C. *Nano Lett.* **2007**, *7*, 1542–1550.
(7) Chithrani, B. D.; Ghazani, A. A.; Chan, W. C. *Nano Lett.* **2006**, *6*, 662–668.
(8) Murray, C. B.; Kagan, C. R.; Bawendi, M. G. *Annu. Rev. Mater. Sci.* **2000**, *30*, 545–610.
(9) Gonzalez, A. L.; Noguez, C.; Ortiz, G. P.; Rodriguez-Gattorno, G. *J. Phys. Chem. B* **2005**, *109*, 17512–17517.
(10) Rodriguez-Gattorno, G.; Diaz, D.; Rendon, L.; Hernandez-Segura, G. O. *J. Phys. Chem. B* **2002**, *106*, 2482–2487.
(11) Corbierre, M. K.; Cameron, N. S.; Sutton, M.; Mochrie, S. G.; Lurio, L. B.; Ruhm, A.; Lennox, R. B. *J. Am. Chem. Soc.* **2001**, *123*, 10411–10412.
(12) Boal, A. K.; Ilhan, F.; DeRouchey, J. E.; Thurn-Albrecht, T.; Russell, T. P.; Rotello, V. M. *Nature* **2000**, *404*, 746–748.
(13) Tatumi, R.; Fujihara, H. *Chem. Commun.* **2005**, (1), 83–85.
(14) Carroll, J. B.; Frankamp, B. L.; Rotello, V. M. *Chem. Commun.* **2002**, (17), 1892–1893.
(15) Terrill, R. H.; Postlethwaite, T. A.; Chen, C.; Poon, C. D.; Terzis, A.; Chen, A.; Hutchison, J. E.; Clark, M. R.; Wignall, G. *J. Am. Chem. Soc.* **1995**, *117*, 12537–12548.
(16) Plech, A.; Kotaidis, V.; Grésillon, S.; Dahmen, C.; von Plessen, G. *Phys. Rev. B* **2004**, *70*, 195423.
(17) Lenggoro, I. W.; Xia, B.; Okuyama, K.; de la Mora, J. F. *Langmuir* **2002**, *18*, 4584–4591.
(18) Sperling, R. A.; Liedl, T.; Duhr, S.; Kudera, S.; Zanella, M.; Lin, C. A. J.; Chang, W. H.; Braun, D.; Parak, W. J. *J. Phys. Chem. C* **2007**, *111*, 11552–11559.
(19) Kuyper, C. L.; Fujimoto, B. S.; Zhao, Y.; Schiro, P. G.; Chiu, D. T. *J. Phys. Chem. B* **2006**, *110*, 24433–24441.
(20) Van Delden, R. A.; Ter Wiel, M. K. J.; Pollard, M. M.; Vicario, J.; Koumura, N.; Feringa, B. L. *Nature* **2005**, *437*, 1337–1340.
(21) Raula, J.; Shan, J.; Nuopponen, M.; Niskanen, A.; Jiang, H.; Kauppinen, E. I.; Tenhu, H. *Langmuir* **2003**, *19*, 3499–3504.
(22) McIntosh, C. M.; Esposito, E. A., III.; Boal, A. K.; Simard, J. M.; Martin, C. T.; Rotello, V. M. *J. Am. Chem. Soc.* **2001**, *123*, 7626–7629.
(23) Tkachenko, A. G.; Xie, H.; Coleman, D.; Glomm, W.; Ryan, J.; Anderson, M. F.; Franzen, S.; Feldheim, D. L. *J. Am. Chem. Soc.* **2003**, *125*, 4700–4701.
(24) Tkachenko, A. G.; Xie, H.; Liu, Y.; Coleman, D.; Ryan, J.; Glomm, W. R.; Shipton, M. K.; Franzen, S.; Feldheim, D. L. *Bioconjugate Chem.* **2004**, *15*, 482–490.
(25) Grant, C. D.; Schwartzberg, A. M.; Norman, T. J., Jr.; Zhang, J. Z. *J. Am. Chem. Soc.* **2003**, *125*, 549–553.
(26) Bogatyrev, V. A.; Dykman, L. A.; Khlebtsov, B. N.; Khlebtsov, N. G. *Opt. Spectrosc.* **2004**, *96*, 128–135.
(27) Kreibig, U.; Vollmer, M. *Optical Properties of Metal Clusters*; Springer: New York, 1995.
(28) Klar, T.; Perner, M.; Grosse, S.; von Plessen, G.; Spirkl, W.; Feldmann, J. *Phys. Rev. Lett.* **1998**, *80*, 4249–4252.
(29) Berciaud, S.; Cognet, L.; Tamarat, P.; Lounis, B. *Nano Lett.* **2005**, *5*, 515–518.
(30) Sönnichsen, C.; Geier, S.; Hecker, N. E.; von Plessen, G.; Feldmann, J.; Ditlbacher, H.; Lamprecht, B.; Krenn, J. R.; Aussenegg, F. R.; Chan, V. Z. H. *Appl. Phys. Lett.* **2000**, *77*, 2949.
(31) Link, S.; El-Sayed, M. A. *Int. Rev. Phys. Chem.* **2000**, *19*, 409–453.
(32) Link, S.; El-Sayed, M. A. *J. Phys. Chem. B* **1999**, *103*, 4212–4217.
(33) Rodriguez-Fernandez, J.; Perez-Juste, J.; Garcia de Abajo, F. J.; Liz-Marzan, L. M. *Langmuir* **2006**, *22*, 7007–7010.
(34) Gaikwad, A. V.; Verschuren, P.; Eiser, E.; Rothenberg, G. *J. Phys. Chem. B* **2006**, *110*, 17437–17443.
(35) Njoki, P. N.; Lim, I. S.; Mott, D.; Park, H.; Khan, B.; Mishra, S.; Sujakumar, R.; Luo, J.; Zhong, C. *J. Phys. Chem. C* **2007**, *111*, 14664–14669.
(36) Sprunken, D. P.; Omi, H.; Furukawa, K.; Nakashima, H.; Sychugov, I.; Kobayashi, Y.; Torimitsu, K. *J. Phys. Chem. C* **2007**, *111*, 14299–14306.
(37) Palpant, B.; Prével, B.; Lermé, J.; Cottancin, E.; Pellarin, M.; Treilleux, M.; Perez, A.; Vialle, J. L.; Broyer, M. *Phys. Rev. B* **1998**, *57*, 1963–1970.
(38) Link, S.; Wang, Z. L.; El-Sayed, M. A. *J. Phys. Chem. B* **1999**, *103*, 3529–3533.

(39) Alvarez, M. M.; Khoury, J. T.; Schaaff, T. G.; Shafigullin, M. N.; Vezmar, I.; Whetten, R. L. *J. Phys. Chem. B* **1997**, *101*, 3706–3712.
(40) Scaffardi, L. B.; Pellegri, N.; Sanctis, O.; Tocho, J. O. *Nanotechnology* **2005**, *16*, 158–163.
(41) Scaffardi, L. B.; Tocho, J. O. *Nanotechnology* **2006**, *17*, 1309–1315.
(42) Lee, K. S.; El-Sayed, M. A. *J. Phys. Chem. B* **2006**, *110*, 19220–19225.
(43) Kelly, K. L.; Coronado, E.; Zhao, L. L.; Schatz, G. C. *J. Phys. Chem. B* **2003**, *107*, 668–677.
(44) Hovel, H.; Fritz, S.; Hilger, A.; Kreibig, U.; Vollmer, M. *Phys. Rev. B* **1993**, *48*, 18178–18188.
(45) Juluri, B. K.; Zheng, Y. B.; Ahmed, D.; Jensen, L.; Huang, T. J. *J. Phys. Chem. C* **2008**, *112*, 7309–7317.
(46) Jain, P. K.; El-Sayed, M. A. *Nano Lett.* **2007**, *7*, 2854–2858.
(47) Norman Jr, T. J.; Grant, C. D.; Magana, D.; Zhang, J. Z.; Liu, J.; Cao, D.; Bridges, F.; Van Buuren, A. *J Phys. Chem. B* **2002**, *106*, 7005–7012.
(48) Amendola, V.; Polizzi, S.; Meneghetti, M. *J. Phys. Chem. B* **2006**, *110*, 7232–7237.
(49) Amendola, V.; Polizzi, S.; Meneghetti, M. *Langmuir* **2007**, *23*, 6766–6770.
(50) Amendola, V.; Meneghetti, M. *J. Mater. Chem.* **2007**, *17*, 4705–4710.
(51) Bosbach, J.; Hendrich, C.; Stietz, F.; Vartanyan, T.; Trager, F. *Phys. Rev. Lett.* **2002**, *89*, 257404.
(52) Garcia, M. A.; de la Venta, J.; Crespo, P.; Lopis, J.; Penadés, S.; Fernández, A.; Hernando, A. *Phys. Rev. B* **2005**, *72*, 241403.
(53) Lica, G. C.; Zelakiewicz, B. S.; Constantinescu, M.; Tong, Y. Y. *J. Phys. Chem. B* **2004**, *108*, 19896–19900.
(54) Johnson, P. B.; Christy, R. W. *Phys. Rev. B* **1972**, *6*, 4370–4379.
(55) Palik, E. D. *Handbook of Optical Constants of Solids*; Academic Press: New York, 1985.
(56) Jensen, T. R.; Schatz, G. C.; Van Duyne, R. P. *J. Phys. Chem. B* **1999**, *103*, 2394–2401.
(57) Li, X.; Tamada, K.; Baba, A.; Knoll, W.; Hara, M. *J. Phys. Chem. B* **2006**, *110*, 15755–15762.
(58) Granqvist, C. G.; Hunderi, O. *Phys. Rev. B* **1977**, *16*, 3513–3534.
(59) Söderlund, J.; Kiss, L. B.; Niklasson, G. A.; Granqvist, C. G. *Phys. Rev. Lett.* **1998**, *80*, 2386–2388.
(60) Granqvist, C. G.; Buhrman, R. *Solid State Commun.* **1976**, *18*, 123–126.
(61) Granqvist, C. G.; Buhrman, R. A. *J. Appl. Phys.* **1976**, *47*, 2200.
(62) Miotello, A.; De Marchi, G.; Mattei, G.; Mazzoldi, P.; Sada, C. *Phys. Rev. B* **2001**, *63*, 75409.

JP8082425